

Connected and disconnected stable regions of solitons of nonlinear Schrödinger equation with \mathcal{PT} -symmetric potential

Niladri Ghosh* and Amiya Das†

Department of Mathematics, University of Kalyani, Kalyani - 741235, WB, India.

Debraj Nath‡

Department of Mathematics, Vivekananda College, Kolkata - 700063, WB, India.

We have considered cubic nonlinear Schrödinger equation along with supersymmetric \mathcal{PT} like potential and obtained exact stationary solutions in terms of bright and bright-dark interacting solitons. The \mathcal{PT} broken and \mathcal{PT} unbroken regions are demonstrated also depicted. Connected and disconnected stable regions of bright and dark solitons are examined incorporating linear stability analysis validated by direct numerical simulations. Moreover, the strength of stability has been illustrated through excitations of bright and dark solitons.

I. INTRODUCTION

A fundamental axiom of quantum mechanics is that every physical observable is associated with a real spectrum and thus operators representing such physical observables must be Hermitian. In quantum mechanics, in order for the energy levels to be real and the theory to be probability conserving (or unitary evolution), it is usually assumed that the Hamiltonian (Schrödinger) operator be Hermitian. In the case of the Hamiltonian operator, this requirement gives rise to real energy levels and the theory guaranteeing conservation of probability. In recent years, in a series of papers by Bender and coworkers [1], a considerable attention has been shown in a weaker version of the Hermiticity axiom in which many non-Hermitian Hamiltonians may also lead to entirely real spectra provided they possess something known as \mathcal{PT} (parity-time) symmetry. The fundamental idea of \mathcal{PT} symmetric quantum mechanics is to replace the concept of Hermitian Hamiltonian by weaker condition that it possess space-time reflection symmetry (\mathcal{PT} -symmetry). The linear space-reflection operator \mathcal{P} , responsible for spatial reflection, is defined through the operations $p \rightarrow -p, x \rightarrow -x$, while the anti-linear time-reversal operator \mathcal{T} leads to $p \rightarrow -p, x \rightarrow x$ and to complex conjugation $i \rightarrow -i$. Dynamical systems are known to be \mathcal{PT} symmetric if they remain invariant under the combined parity \mathcal{P} and time-reversal \mathcal{T} transformation. A necessary condition for a Hamiltonian to be \mathcal{PT} symmetric is that the potential function $V_{\mathcal{PT}} = V(x) + iW(x)$ should satisfy the condition $V_{\mathcal{PT}}(x) = V_{\mathcal{PT}}^*(-x)$, with $*$ denoting the complex conjugation. A \mathcal{PT} symmetric system exhibits entirely real spectra as long as the robustness of the imaginary component of the complex potential is less than a certain threshold value. The corresponding system undergoes a drastic phase transition also known as spontaneous \mathcal{PT} symmetry breaking [2] on exceeding the threshold value. The \mathcal{PT} symmetric wave propagation in optical structures can be replaced by the complex refractive index and balanced gain-loss profile which was judiciously predicted through the experimental execution in optical metamaterials, synthetic photonic lattices, microring lasers and optically induced atomic lattices etc [3]. Though the theory was initially originated in quantum mechanics, but later on the concept of \mathcal{PT} symmetry has also found applications in different fields, e.g., optics [4–8], electronics [9], Bose-Einstein conden-

sation [10–12], metamaterials [13–17], etc. Furthermore \mathcal{PT} symmetry has been realized experimentally [18–21].

In the last decades, the theory of existence of nonlinear localized modes in \mathcal{PT} symmetric potential and their linear stability has been studied very promptly [22, 23]. Several interesting potentials for example Scarf-II potential [24], harmonic potential [25], Rosen-Morse potential [26], Gaussian potential [27–32], sextic anharmonic double-well potential [33], time-dependent harmonic-Gaussian potential [34] etc are considered for study.

The nonlinear Schrödinger equation (NLSE) is one of the pioneer mathematical model which arises in diversified physical systems. This equation is a key model describing wave processes in plasma physics, Bose-Einstein condensates (BEC), gravitational models for quantum mechanics, wave propagation in biological and geological systems [35] and nonlinear optics [36]. In some of these fields and many others, the NLS equation appears as an asymptotic limit for a slowly varying dispersive wave envelope propagating in a nonlinear medium. It also plays an important role in describing full spatiotemporal optical solitons or light bullets in the theory of nonlinear optics [36]. During the past few years, exact solutions of NLSE with \mathcal{PT} symmetric potentials and their stability have been studied by many authors since they are useful in different contexts [26, 37–56]. In Ref.[54], the exact stationary solutions of derivative nonlinear Schrödinger equation have been obtained in presence of a \mathcal{PT} symmetric potential as a sum of super-Gaussian and parabolic potentials. The theory of supersymmetry and deformed supersymmetry are used in [55, 56] to retrieve exact analytical localized solutions in context of a number of complex \mathcal{PT} symmetric potentials and supersymmetric potentials along with power law nonlinearity.

As we know that, a pair of potentials $V_{\pm}(x)$ are said to be supersymmetric, if there exists a function $U(x)$ such that, $V_{\pm}(x) = U^2(x) \pm U'(x)$ [57]. In this paper, we have considered $(a, v_0, w_0, U(x))$, where $U(x) = U_R(x) + iU_I(x)$ such that,

$$\begin{aligned} V &= v_0 \operatorname{Re}(U^2 - U') = v_0 (U_R^2 - U_I^2 - U'_R), \\ W &= w_0 \operatorname{Im}(U^2 - U') = w_0 (2U_R U_I - U'_I), \end{aligned} \quad (1)$$

v_0 and w_0 are amplitudes of real and imaginary parts of the potential, with $w_0 \neq 0$ and a is a real constant, which will be connected to solutions of a NLSE. Then the functions U_R and U_I satisfy \mathcal{PT} -symmetric conditions

$$U_R(x) = -U_R(-x), \quad U_I(x) = U_I(-x), \quad (2)$$

and a cubic nonlinear Schrödinger equation has exact solutions for deformed supersymmetric potential $V(x) + iW(x)$.

* Email: niladri.02mgf@gmail.com

† Email: amiya620@gmail.com

‡ Corresponding author. Email: debrajn@gmail.com

The optical solitons are classified into two forms based on the sign of group velocity dispersion. Solitons in negative dispersion regime are known as bright solitons (BS) and solitons in positive dispersion regime are called dark solitons (DS). Dark soliton can be stressed as a localized pulse appearing as an acute dip on the background of continuous wave. On the other hand, bright soliton appears as a crest above the continuous wave. Recently, in a series of paper [58], the existence of dark solitons are verified experimentally in the area of nonlinear fiber optics, plasma, BEC and waveguide arrays. In most of the cases, cubic NLSE has either a bright or dark soliton. In this paper, we will find two solutions of a cubic NLSE and they will be the ground and first excited states of linear Schrödinger equation. In this paper, we will investigate stability analysis of BS and DS of a cubic nonlinear Schrödinger equation with deformed supersymmetric potential. Then we will find stable regions of BS and DS and regions will be verified by different numerical methods. Finally, regions will be checked by excitations of BS and DS of a cubic time dependent NLSE.

The rest of the paper is structured as follows. In Sec. II, we will obtain exact stationary solutions in terms of BS and bright-dark soliton interaction of a cubic nonlinear Schrödinger equation along with complex \mathcal{PT} symmetric potential. In Sec. III, linear stability analysis is illustrated incorporating direct numerical simulations, which assures about stable behavior of BS and DS depending on potential parameters. Also, excitations of nonlinear BS and DS of a time dependent NLSE and some numerical results have been reported in Sec. IV. Finally, conclusions have been drawn in Sec. V.

II. METHODOLOGY

Let us consider a cubic NLSE

$$i\Psi_t = -\Psi_{xx} + (V(x) + iW(x))\Psi + g|\Psi|^2\Psi \quad (3)$$

with a complex \mathcal{PT} -symmetric potential $V(x) + iW(x)$, where g is the nonlinearity parameter. To solve Eq.(3) a transformation

$$\Psi(x, t) = e^{-i\mu t}\psi(x) \quad (4)$$

is considered, where μ is a real propagation constant. Then from Eq.(3) one can obtain

$$-\frac{d^2\psi}{dx^2} + (V + iW)\psi + g|\psi|^2\psi = \mu\psi \quad (5)$$

and it has a solution of the form $C_0 e^{-\int(U_R+i a U_I)dx}$, $a \in \mathbb{R}$. In particular if, $(a, v_0, w_0, U) = (1, 1, 1, U)$ and $g = 0$, then the NLSE reduces to a LSE with exact supersymmetric potentials with zero energy normalized solution $e^{-\int(U_R+i U_I)dx}$. In this paper we will find solutions of NLSE (5) as well as (3), where $(a, v_0, w_0) \neq (1, 1, 1)$.

A. Solution 1

A solution of Eq.(5) is taken to be of the form

$$\psi_0 = C_0 e^{-\int(U_R+i a U_I)dx}, \quad \mu = \mu_0 \quad (6)$$

where C_0 is the amplitude and $\lim_{|x| \rightarrow \infty} |\psi_0(x)| = 0$. Now substituting Eq.(6) into Eq.(5) and equating real and imaginary

parts, we obtain [55]

$$\begin{aligned} (v_0 - 1) \left(U_R^2 - U_R' \right) + (a^2 - v_0) U_I^2 \\ + g C_0^2 e^{-2 \int U_R(x) dx} = \mu_0, \\ \left(2U_R U_I - U_I' \right) (w_0 - a) = 0. \end{aligned} \quad (7)$$

If $2U_R U_I - U_I' = 0$, then \mathcal{PT} -symmetric potential becomes real potential. In this paper we have considered $w_0 = a$ and therefore (a, v_0, w_0, U) exists which satisfy relations of (7) and solution (6) exists.

B. Solution 2

If possible let, there be another solution of the form

$$\psi_1(x) = C_1 e^{-\int(U_R + i a U_I) dx} F(x), \quad \mu = \mu_1, \quad (8)$$

where $\lim_{|x| \rightarrow \infty} |\psi_1(x)| \neq 0$. Using Eq.(8) into Eq.(5), we obtain

$$\begin{aligned} -F'' + 2(U_R + i a U_I) F' \\ + g \{ C_1^2 |F|^2 - C_0^2 \} e^{-2 \int U_R dx} F = (\mu_1 - \mu_0) F. \end{aligned} \quad (9)$$

Eq.(9) is the additional condition for existence of solution of Eq.(8). In particular, $g = 0$, then conditions are

$$\begin{aligned} (v_0 - 1) \left(U_R^2 - U_R' \right) + (a^2 - v_0) U_I^2 = \mu_0, \\ \left(2U_R U_I - U_I' \right) (w_0 - a) = 0, \\ -F'' + 2(U_R + i a U_I) F' = (\mu_1 - \mu_0) F. \end{aligned} \quad (10)$$

Eq.(10) has the solution $(a, v_0, w_0) = (1, 1, 1)$ and F satisfies the relation

$$-F''(x) + 2U(x)F'(x) = \mu_1 F(x), \quad (11)$$

which has infinitely many solutions depends on $U(x)$. In this paper, we will find solution of (9) by an example. Then the NLSE (3) has two solutions of the forms (6) and (8). The solution (13) is a BS and the solution (14) may be BS or DS.

C. Example

Let us choose $U_R(x) = \tanh x$, $U_I(x) = \beta \operatorname{sech} x$, where β is a real constant. Then \mathcal{PT} -symmetric potential $V(x) + iW(x)$ is defined by

$$\begin{aligned} V(x) = v_0 - v_0(2 + \beta^2) \operatorname{sech}^2 x, \\ W(x) = 3w_0\beta \operatorname{sech} x \tanh x. \end{aligned} \quad (12)$$

This potential is known as \mathcal{PT} -symmetric Scarf potential [57]. In Fig. 1, we have plotted real and imaginary parts of the potential, for different values of parameters and the parameters are taken from \mathcal{PT} broken and unbroken region of the linear Schrödinger equation with this complex potential. In Sec. IID, the \mathcal{PT} broken and unbroken symmetry are discussed. It is to be noted that, this potential was considered within the context of cubic NLSE [4, 26, 37, 38, 40, 46, 50, 52, 55, 56, 59]. Then solution 1 is given by

$$\Psi_0(x, t) = C_0 \operatorname{sech} x e^{-i w_0 \beta \tan^{-1}(\sinh x) - i \mu_0 t}, \quad (13)$$

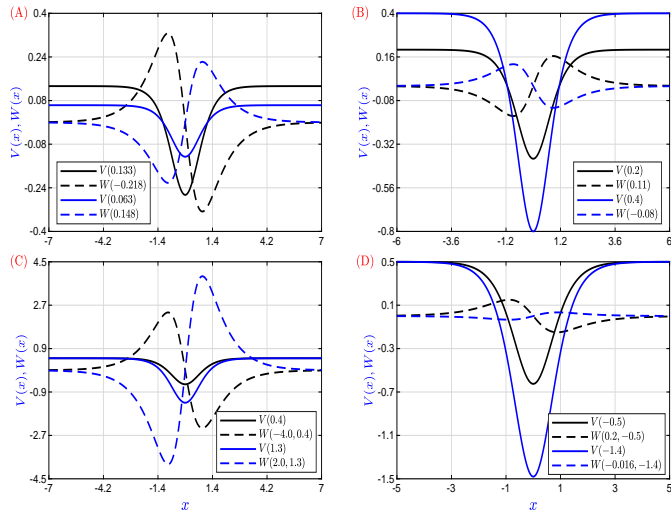


FIG. 1. Plot of real and imaginary parts of \mathcal{PT} -symmetric potential (12). Parameters are (A) black lines $v_0 = 0.133, \beta = 1, w_0 = -0.218$ and blue lines $v_0 = 0.063, \beta = 1, w_0 = 0.148$; (B) black lines $v_0 = 0.2, \beta = 1, w_0 = 0.11$ and blue lines $v_0 = 0.4, \beta = 1, w_0 = -0.08$; (C) black lines $v_0 = 0.5, \beta = 0.4, w_0 = -4$ and blue lines $v_0 = 0.5, \beta = 1.3, w_0 = 2$; (D) black lines $v_0 = 0.5, \beta = -0.5, w_0 = 0.2$ and blue lines $v_0 = 0.5, \beta = -1.4, w_0 = -0.016$.

and solution 2 is given by

$$\Psi_1(x, t) = C_1 (\gamma \operatorname{sech} x + i\delta \tanh x) e^{-i w_0 \beta \tan^{-1}(\sinh x) - i\mu_1 t}, \quad (14)$$

where

$$\mu_0 = v_0 - 1, \quad C_0 = \left\{ \frac{v_0(2 + \beta^2) - w_0^2 \beta^2 - 2}{g} \right\}^{\frac{1}{2}}, \quad (15)$$

and

$$\begin{aligned} \mu_1 &= v_0 + \frac{v_0(2 + \beta^2) - w_0^2 \beta^2 - 2}{4\beta^2 w_0^2 - 1}, \\ C_1 &= \left\{ \frac{v_0(2 + \beta^2) - w_0^2 \beta^2 - 2}{g\delta^2(4\beta^2 w_0^2 - 1)} \right\}^{\frac{1}{2}}, \\ \gamma &= -2\beta\delta w_0. \end{aligned} \quad (16)$$

We have plotted real and imaginary parts of solution (13) in Fig. 2 and of solution (14) in Fig. 3 for different set of parameters. It is to be noted that, for Fig. 2 and Fig. 3, all parameters are taken from \mathcal{PT} broken stable, \mathcal{PT} broken unstable and \mathcal{PT} unbroken stable, \mathcal{PT} unbroken unstable regions of Fig. 6, 7 and 8. We observe that, solution (13) is a BS and solution (14) is a BS, if $w_0^2 > \frac{1}{4\beta^2}$ and a DS, if $w_0^2 < \frac{1}{4\beta^2}$. Therefore, the phase transition between BS and DS is occurred for the solution (14) at the points on the curve $w_0^2 = \frac{1}{4\beta^2}$. Now, we will focus on LSE with complex potential (12).

D. Spectrum of linear Schrödinger equation

We first consider the linear spectrum of L with \mathcal{PT} -symmetric potential (12) as

$$\begin{aligned} L\psi(x) &= \mu\psi, \\ L &\equiv -\frac{d^2}{dx^2} + V(x) + iW(x), \end{aligned} \quad (17)$$

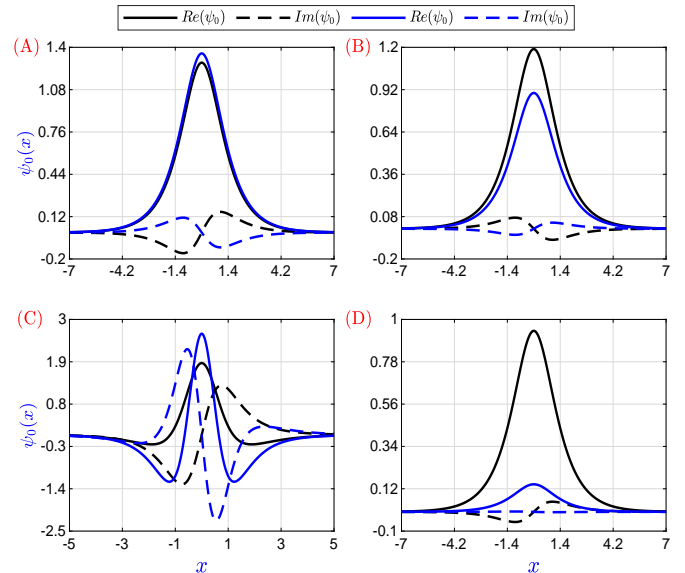


FIG. 2. Plot of real and imaginary parts of (13). The parameters are taken from (A) stable \mathcal{PT} broken region: for black lines $v_0 = 0.133, w_0 = -0.218$ and for blue lines $v_0 = 0.063, w_0 = 0.148$; (B) stable \mathcal{PT} unbroken region: for black lines $v_0 = 0.2, w_0 = 0.11$ and for blue lines $v_0 = 0.4, w_0 = -0.08$; (C) unstable \mathcal{PT} broken region: for black lines $\beta = 0.4, w_0 = -4.0$ and for blue lines $\beta = 1.3, w_0 = 2.0$, (D) stable \mathcal{PT} unbroken region: for black lines $\beta = -0.5, w_0 = 0.2$ and for blue lines $\beta = -1.4, w_0 = -0.016$. All regions are shown in Fig. 6.

where μ is the eigenvalue and $\psi(x)$ is the corresponding eigenfunction. For the bound states $\lim_{x \rightarrow \infty} |\psi(x)| \rightarrow 0$. Now spectrum of the linear operator L with complex \mathcal{PT} -symmetric potential (12) may be real or complex conjugates. Then, one can find v_0, w_0, β , for which linear operator has real spectrum and it is possible, if [60]

$$3|w_0\beta| \leq \frac{1}{4} + v_0(2 + \beta^2). \quad (18)$$

Fig. 4 exhibits \mathcal{PT} symmetry broken and unbroken phase transition of the complex potential (12). The region on and above the surface of Fig. 4 is \mathcal{PT} unbroken and the region below the surface is \mathcal{PT} broken. The imaginary parts of some eigen values of the linear operator L (17) are shown in Fig. 5, in (w_0, v_0) plane for $\beta = 1$ and in (w_0, β) plane for $v_0 = 0.5$. From Fig. 4 one can find a suitable set of parameters for which the potential is \mathcal{PT} unbroken and the spectrum of operator L are real. First of all under this set of parameters, we will investigate the linear stability analysis of solutions (13) and (14) and we denote this point by P_1 and then we will investigate further for another set of parameters, which is denoted by P_2 . Next, we will investigate their stability analysis for collection of points joining P_1 and P_2 by a curve in (w_0, v_0) plane for fixed β and in (w_0, β) plane for fixed v_0 in the next Sec. III.

III. LINEAR STABILITY ANALYSIS

One of the most important property of solutions of NLSE is their stability. Here we will examine linear stability of solutions of a NLSE. To this end, solution in Eq.(4) is given small perturbations $v(x), w(x)$ and is taken to be of the form

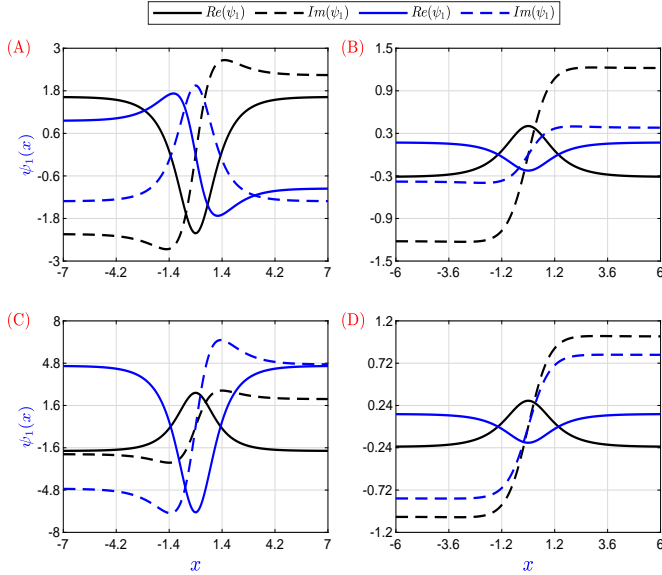


FIG. 3. Plot of real and imaginary parts of (14). The parameters are taken from (A) unstable \mathcal{PT} broken region: (black lines) $v_0 = -0.2, w_0 = 0.40$ and (blue lines) $v_0 = 0.4, w_0 = -0.45$; (B) stable \mathcal{PT} unbroken region: (black lines) $v_0 = 0.20, w_0 = -0.16$ and (blue lines) $v_0 = 0.65, w_0 = 0.27$; (C) unstable \mathcal{PT} broken region: (black lines) $\beta = 0.23, w_0 = -2.00$ and (blue lines) $\beta = 0.29, w_0 = 1.70$, (D) stable \mathcal{PT} unbroken region: (black lines) $\beta = -0.10, w_0 = 1.40$ and (blue lines) $\beta = -0.85, w_0 = -0.13$. All the regions are shown in Fig. 8.

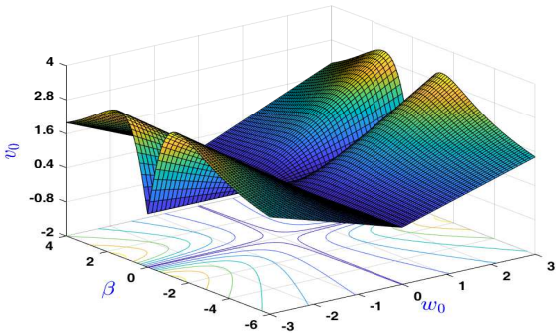


FIG. 4. Plot of \mathcal{PT} -symmetric phase diagram of v_0 of the linear operator (17) with respect to w_0 and β .

[61–65]

$$\Psi(x, t) = \{\psi(x) + [\tilde{v}(x) + \tilde{w}(x)] e^{\lambda t} + [\tilde{v}^*(x) - \tilde{w}^*(x)] e^{\lambda^* t}\} e^{i\mu t}, \quad (19)$$

where the superscript $*$ represents the complex conjugation, $|v|, |w| \ll 1$ are infinitesimal normal mode perturbation eigenfunctions, which may grow during propagation with the perturbation growth rate λ . Now substituting the above expression in Eq.(3) and linearizing, one gets the following coupled set of eigenvalue problem:

$$i \begin{pmatrix} h_0 & \nabla^2 + h_1 \\ \nabla^2 + h_2 & h_3 \end{pmatrix} \begin{pmatrix} \tilde{v} \\ \tilde{w} \end{pmatrix} = \lambda \begin{pmatrix} \tilde{v} \\ \tilde{w} \end{pmatrix}, \quad (20)$$

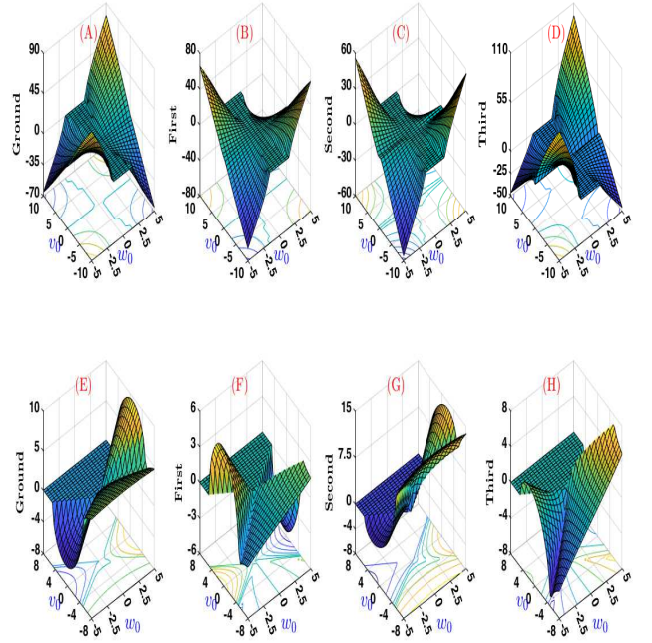


FIG. 5. Plot of imaginary parts of some eigen values of (17), for (A)-(D) $v_0 = 0.5$ and for (E)-(H) $\beta = 1$.

where

$$\begin{aligned} h_0 &= \frac{g}{2} (\psi^2 - \psi^{*2}) + i W(x), \\ h_1 &= -\mu + V(x) + g|\psi|^2 + g \left\{ |\psi|^2 - \frac{1}{2} (\psi^2 + \psi^{*2}) \right\}, \\ h_2 &= -\mu + V(x) + g|\psi|^2 + g \left\{ |\psi|^2 + \frac{1}{2} (\psi^2 + \psi^{*2}) \right\}, \\ h_3 &= -\frac{g}{2} (\psi^2 - \psi^{*2}) + i W(x). \end{aligned} \quad (21)$$

The linear stability is determined by the nature of the eigenvalue problem (20). If there exists any λ with a positive real part, then the perturbed solution will grow exponentially with t resulting in unstable mode. On the other hand, mode is completely stable only when, real parts of λ are not positive. The BS and DS are satisfying boundary conditions

$$\begin{aligned} |\Psi_0(x, t)| &\rightarrow 0, |x| \rightarrow \infty, t > 0, \\ \frac{\partial}{\partial x} \Psi_0(x, t) &\rightarrow 0, |x| \rightarrow \infty, t > 0, \end{aligned} \quad (22)$$

$$\begin{aligned} |\Psi_1(x, t)| &\rightarrow C_1 |\delta|, |x| \rightarrow \infty, t > 0, w_0^2 < \frac{1}{4\beta^2}, \\ \frac{\partial}{\partial x} \Psi_1(x, t) &\rightarrow 0, |x| \rightarrow \infty, t > 0. \end{aligned} \quad (23)$$

In this paper, we will apply the Fourier collocation method (FCM) and finite difference method (FDM) for finding eigenvalues of Eq.(20) for BS and DS respectively. The simulation of these two solutions are obtained by pseudospectral method and finite difference method. Using the definition of power and the VK stability condition [66], one can say that, BS defined in (13) is stable, if $g > 0$ and unstable, if $g < 0$, for the real potential i.e., when $w_0 = 0$. The stable region of BS and DS can not be defined for arbitrary values of v_0, w_0 and β . Therefore, we will find stable regions in (w_0, v_0) plane for fixed β and in (w_0, β) plane for fixed v_0 by applying some numerical techniques.

A. Numerical method

All the special grid points are defined by $x_j = -L + \delta x j$, $j = 1, 2, 3, \dots, N + 1$ (L being the half-width), where $\delta x = 2L/N$ is taken to be the lattice spacing (resolution). The left and right boundary points are denoted by $j = 1$ and $j = N + 1$, respectively. The boundary conditions for BS and DS at the end points are given by

$$|\Psi_0(\pm L, t)| = 0, \quad [\partial_x \Psi_0(x, t)]_{x=\pm L} = 0, \quad (24)$$

and

$$|\Psi_1(\pm L, t)| = C_1 |\delta|, \quad [\partial_x \Psi_1(x, t)]_{x=\pm L} = 0, \quad w_0^2 < \frac{1}{4\beta^2}. \quad (25)$$

In this paper, we will consider two finite difference methods for discretizing Eqs. (3), (24) and (25). For BS (13), we will apply (i) pseudospectral method for second-order spatial derivatives and 4th order Runge-Kutta (RK4) for the temporal derivative and (ii) second-order central-difference formula for second-order spatial derivatives and Crank-Nicholson finite difference method for the temporal derivative. Similarly, for DS we will apply (iii) second-order central-difference formula for second-order spatial derivatives and 4th order Runge-Kutta (RK4) for the temporal derivative and (iv) second-order central-difference formula for second-order spatial derivatives and Crank-Nicholson finite difference method for the temporal derivative [67]. Then, a solution will be considered a stable mode, if none of eigen frequencies $\lambda = \lambda_R + i\lambda_I$ has a positive real part λ_R . Finally, the stable regions will be obtained from the eigenvalue problem (20) and they will be checked by direct dynamical evolution of the NLSE (3) forward with respect to t . To validate linear stability, we will add random noise perturbation for stable mode add eigen vector $(\tilde{v}, \tilde{w})^T$ of (20), which corresponds to largest positive real part λ_R for unstable mode to initial solution. The random numbers are generated from (0, 1).

B. Stability of BS

We now consider two cases of g . In the first one, $g = -1$, the existence of the solution (13) of the NLSE (5) in (w_0, v_0) and (w_0, β) planes are shown in Fig. 6 (A) -(B). The space (w_0, v_0) is divided into seven regions I_i , $i = 1 - 5$, J_1 and J_2 . In region I_1 , solution (13) does not exist. In addition, \mathcal{PT} symmetric phase transition is shown in Fig. 6 (A). In green region $(I_5 \cup J_1 \cup J_2)$ linear operator L (17) is \mathcal{PT} broken and in white region $(\cup_{i=1}^4 I_i)$ L is \mathcal{PT} unbroken. The stable region for solution (13) is shown in Fig. 6 (A) and it is bounded by blue and red curves, which is equal to $I_3 \cup J_1 \cup J_2$. From this figure it is clear that I_3 is \mathcal{PT} unbroken stable, whereas $J_1 \cup J_2$ is \mathcal{PT} broken stable, which is very small with respect to I_3 and total stable region $I_3 \cup J_1 \cup J_2$ is connected. The (w_0, β) space is divided into nine regions $(I_i, i = 1 - 9)$ and they are shown in Fig. 6 (B). From this figure one can see that, solution (13) does not exist in $I_3 \cup I_9$. The linear operator (17) is \mathcal{PT} broken in green region $(I_1 \cup I_5)$, whereas it is unbroken in white region $((\cup_{i=2}^4 I_i) \cup (\cup_{j=6}^9 I_j))$. It is interesting to observe that solution (13) is stable in a connected region I_7 , which entirely lies in \mathcal{PT} unbroken and there is no stable \mathcal{PT} broken mode. [64, 65]. In the second case $g = 1$, the existence of BS in (w_0, v_0) and (w_0, β) planes are shown in Fig. 7 (A) and (C). From Fig. 7 (A) we see that, BS does not exist below the red curve and the operator

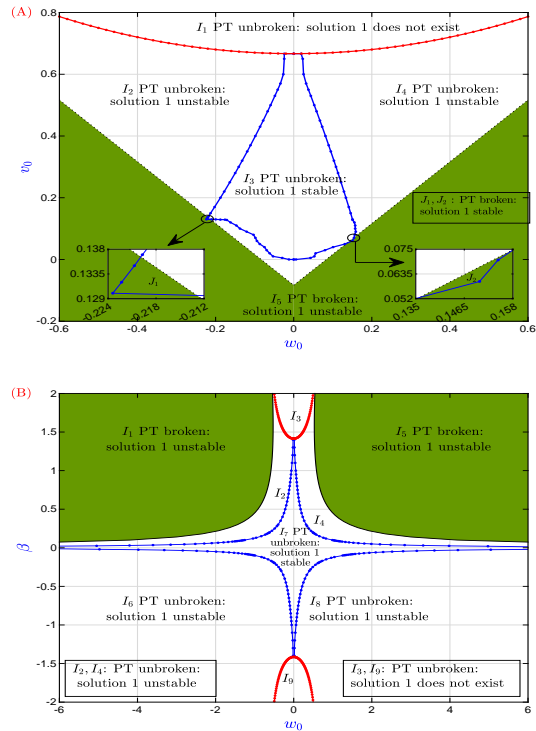


FIG. 6. (A) \mathcal{PT} -symmetric phase transitions of the linear operator (17) with potential (12) and stable-unstable regions of the solution (13) in (w_0, v_0) plane, for $g = -1, \beta = 1.0$. (B) The phase transitions for the same linear operator in (w_0, β) plane and stable-unstable mode of the solution (13) in (w_0, β) plane, for $g = -1, v_0 = 0.5$.

L of (17) is broken in green region, which is entirely below the red curve. BS is stable in two disjoint regions J_1 and $J_2 \subset I_1$ and they are shown in Fig. 7 (B). From Fig. 7 (C) we see that, BS exists in I_2 which is the upward interior of the red parabola and in I_5 which is the downward interior of red parabola. The stable regions exist in four small parts such as $J_3, J_4 \subset I_2$ and $J_5, J_6 \subset I_5$ and they are shown in Fig. 7 (D) and (E). All parts are connected but $\cup_{i=3}^6 J_i$ is disconnected. For $g = 1$, stable region in both planes are very small, which agree with [46].

C. Stability of DS

For $g = -1$ the DS is stable in small region in (w_0, v_0) and (w_0, β) planes satisfying $w_0^2 < \frac{1}{4\beta^2}$ and some additional conditions. In particular, $\beta = 1, \delta = 1$, we have found a stable region in (w_0, v_0) plane, such that $\frac{2+w_0^2}{3} \leq v_0 \leq \frac{2+w_0^2}{3} + \epsilon$, where $0 < \epsilon < 0.1$. We now consider the second case $g = 1$, DS exists in a domain which lies between two vertical lines $w_0^2 < \frac{1}{4\beta^2}$ and a parabolic curve $v_0 < \frac{w_0^2 \beta^2 + 2}{\beta^2 + 2}$ in (w_0, v_0) plane. In particular, for $\beta = 1, \delta = 1$, the region is shown in Fig. 8 (A) and the linear operator is broken in green region $\cup_{i=5}^7 I_i$. Stable modes of DS are marked by *blue dots*, I_3 and *magenta dots*, I_4 represent unstable modes. It is to be found that, stable modes are exist within \mathcal{PT} unbroken region. We did not find stable mode in broken region after several trials. Similarly, existence of (14) and \mathcal{PT} broken-unbroken phase transition shown in Fig. 8 (B) in (w_0, β) plane, for $v_0 = 0.5, \delta = 1$. The space (w_0, β) is divided into eleven regions $I_i, i = 1 - 11$. The linear operator L is broken in

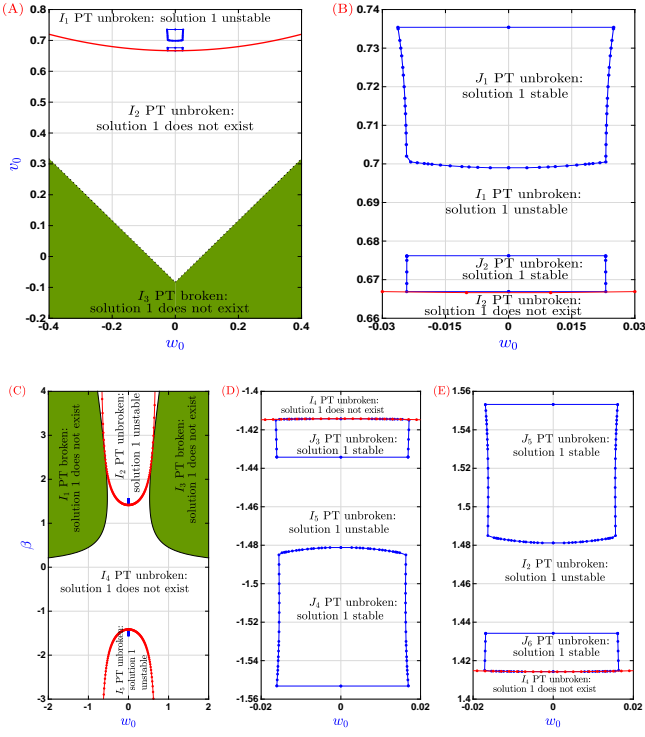


FIG. 7. (A) Phase transition of the linear operator (17) with potential (12) and stable-unstable mode of the solution (13) in (w_0, v_0) plane for $g = 1, \beta = 1$. (C) The phase transitions for the same linear operator and stable-unstable mode of the solution (13) in (w_0, β) plane, for $g = 1, v_0 = 0.5$.

$I_5 \cup I_6 \cup I_9 \cup I_{10}$ and unbroken in $\cup_{i=1}^4 I_i \cup I_7 \cup I_8 \cup I_{11}$ and DS exists in a region bounded by red curves. Stable modes of DS are marked by *blue dots*, I_8 and unstable in $\cup_{i=1}^7 I_i$. The DS has stable modes only in \mathcal{PT} unbroken region. To confirm all these stable modes of BS and DS, we will investigate their excitations in the next section IV.

IV. EXCITATION

Now, we will focus on nature of solutions of time dependent NLSE with complex \mathcal{PT} -symmetric potential

$$i \Psi_t = -\Psi_{xx} + (V(x, t) + iW(x, t)) \Psi + g|\Psi|^2 \Psi, \quad (26)$$

where $V(x, t), W(x, t)$ are given by Eq.(12) with $v_0 \rightarrow v_0(t)$ and $w_0 \rightarrow w_0(t)$ satisfy [68]

$$\{v_0, w_0, \beta\}(t) = \begin{cases} (\{v_{02}, w_{02}, \beta_{02}\} - \{v_{01}, w_{01}, \beta_{01}\}) f(t) \\ + \{v_{01}, w_{01}, \beta_{01}\}, 0 \leq t \leq 5000 \\ \{v_{02}, w_{02}, \beta_{02}\}, t > 5000 \end{cases}, \quad (27)$$

where f is a real valued function of t . It is easy to verify that, solutions (13) and (14) do not satisfy Eq.(26) but they satisfy for initial time $t = 0$ and $t \geq 5000$. In this paper we have considered $f(t) = \sin \frac{\pi t}{10000}$, $0 \leq t \leq 5000$.

A. Excitation of BS

We have displayed excitations of BS of (26), with initial condition (13) in Fig. 9 (C) -(F), for $g = -1$ along four curves $C_1 - C_4$. Each curve has initial point $P_1(w_{01}, v_{01})$

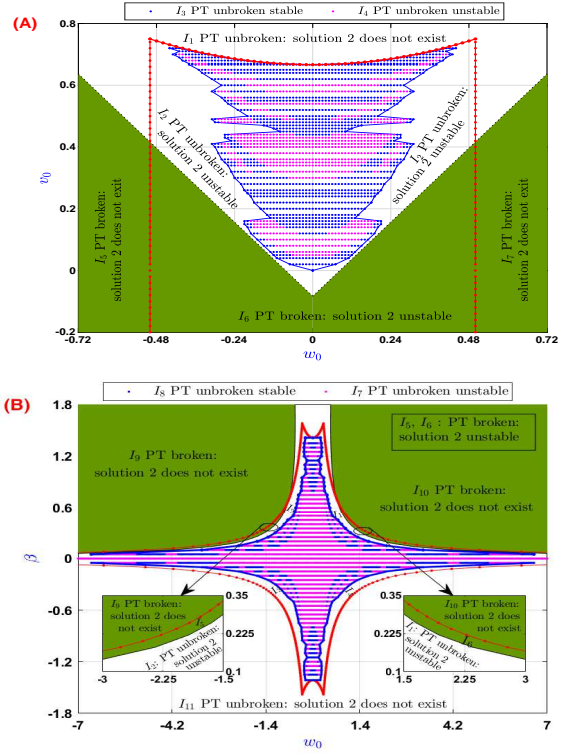


FIG. 8. (A) Phase transition of the linear operator L (17) with potential (12) and stable-unstable mode of the solution (14) in (w_0, v_0) plane, $g = 1, \beta = 1, \delta = 1$. (B) Phase transition of the same linear operator and stable-unstable mode of the solution (14) in (w_0, β) plane, for $g = 1, v_0 = 0.5, \delta = 1$.

and final point $P_2(w_{02}, v_{02})$. The time dependent potential amplitudes $\min\{v_{01}, v_{02}\} \leq v_0(t) \leq \max\{v_{01}, v_{02}\}$ and $\min\{w_{01}, w_{02}\} \leq w_0(t) \leq \max\{w_{01}, w_{02}\}$ satisfy the Eq.(27) and they are plotted in Fig. 9 (A) with respect to t and the corresponding locus of $(w_0(t), v_0(t))$ for $0 \leq t \leq 5000$, represent curves C_j , $j = 1, 2, 3, 4$ and they are shown in Fig. 9 (B). The curve $C_1 : P_2(-0.22, 0.1335) \curvearrowright P_1(0.15, 0.062)$ is started from $P_1(\in J_2, \text{broken region})$ to $P_2(\in J_1, \text{broken region})$ via unbroken region (I_3), whereas $C_2 : P_2(-0.22, 0.1335) \leftarrow P_1(-0.02, 0.1335)$ is started from $P_1(\in I_3, \text{unbroken region})$ to $P_2(\in J_1, \text{broken region})$. Therefore, excitation Fig. 9 (C) started from a broken point passes through unbroken region and then ended to a broken point, whereas, excitation Fig. 9 (D) started from an unbroken point and then going to broken region. On the otherhand Fig. 9 (E) and (F) are excitations along $C_3 : P_1(-0.08, 0.08) \nearrow P_2(0.022, 0.53)$ and $C_4 : P_1(-0.08, 0.08) \rightarrow P_2(0.022, 0.08)$ and they lie within unbroken region I_3 . One can see that, curves C_1, C_3 are look like oblique whereas, C_2, C_4 are like horizontal but their directions are different and all excitations in (w_0, v_0) plane are stable. We have checked that, BS is stable for all $(w_0, v_0) \in I_3 \cup J_1 \cup J_2$ and its excitation is stable along any curve in any direction which lies in $I_3 \cup J_1 \cup J_2$. Similarly, in (w_0, β) plane for $g = -1, v_0 = 0.5$ excitations of (26) with initial solution (13) are shown in Figs. 10 (A) -(D) along four curves ($C_5 : P_1(-0.017, -1.3) \nearrow P_2(0.017, 1.3)$; $C_6 : P_1(-0.017, -1.3) \uparrow P_2(-0.017, 1.3)$; $C_7 : P_1(-4.7, -0.02) \nearrow P_2(4.7, 0.02)$; $C_8 : P_1(-4.7, -0.02) \rightarrow P_2(4.7, -0.02)$). From Figs. 10 (A) -(D), one can see that BS and its excitations are stable. We observe that, excitation of BS of (26) with initial state (13) is stable along any curve in any direction which lies in \mathcal{PT} unbroken region I_7 of Fig. 6

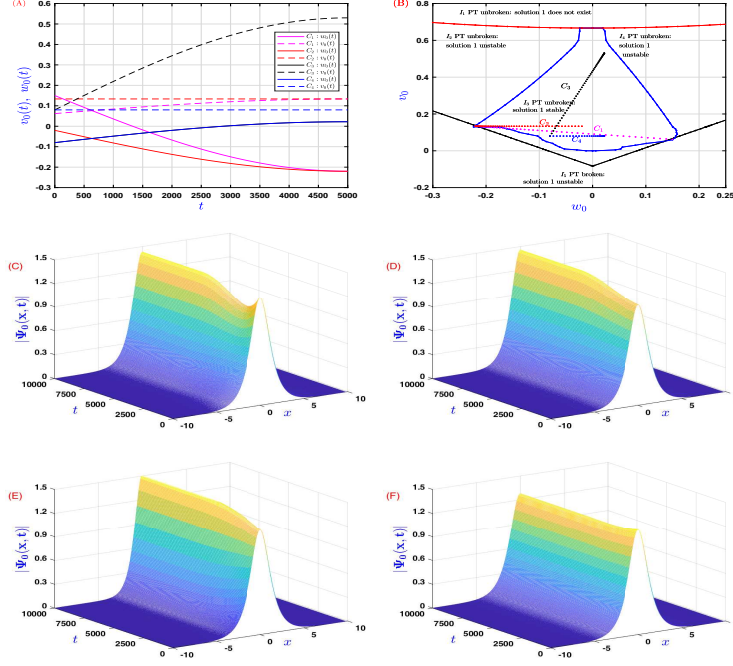


FIG. 9. (A) Shows time dependent potential amplitudes w_0, v_0 for different curves. (B) Shows that stable and unstable regions of BS and four curves C_i , $i = 1 - 4$. Excitations of stable nonlinear localized state of (26) with initial condition (13), for $g = -1$, $\beta = 1$, (C) $v_{01} = 0.062, v_{02} = 0.1335, w_{01} = 0.15, w_{02} = -0.22$ (D) $v_{01} = 0.1335, v_{02} = 0.1335, w_{01} = -0.02, w_{02} = -0.22$ (E) $v_{01} = 0.08, v_{02} = 0.53, w_{01} = -0.08, w_{02} = 0.022$ (F) $v_{01} = 0.08, v_{02} = 0.08, w_{01} = -0.08, w_{02} = 0.022$.

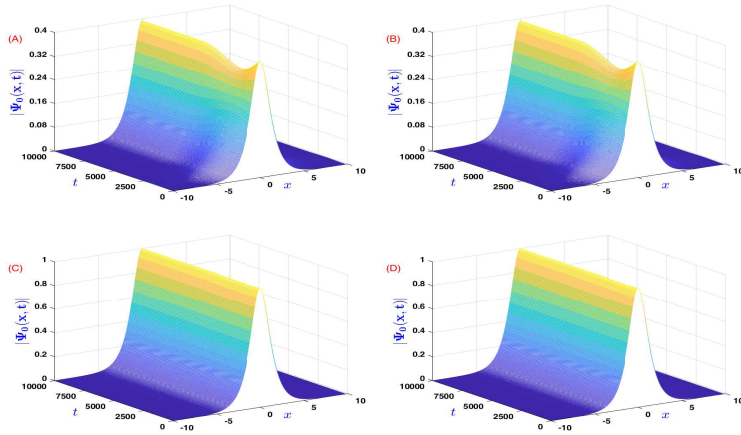


FIG. 10. Excitations of stable nonlinear localized state of (26) with initial condition (13), for $g = -1$, $v_0 = 0.5$, (A) $\beta_{01} = -1.30, \beta_{02} = 1.30, w_{01} = -0.017, w_{02} = 0.017$ (B) $\beta_{01} = -1.30, \beta_{02} = 1.30, w_{01} = -0.017, w_{02} = -0.017$ (C) $\beta_{01} = -0.02, \beta_{02} = 0.02, w_{01} = -4.7, w_{02} = 4.7$ (D) $\beta_{01} = -0.02, \beta_{02} = -0.02, w_{01} = -4.7, w_{02} = 4.7$.

(B) in (w_0, β_0) plane. Similarly, in (w_0, v_0) for $g = 1$, excitations of BS with same initial condition (13) along $C_9 : P_2(-0.024, 0.731) \leftarrow P_1(0.024, 0.731) (\in J_1)$ and $C_{10} : P_1(0.024, 0.731) (\in J_1) \rightarrow P_2(0.076, 0.731)$ are shown in Fig. 11 (A) and (B) respectively. The curve C_9 lies in the stable region J_1 of Fig. 7 (B) and the curve C_{10} is started from a stable point of J_1 and to an unstable point of I_1 of Fig. 7 (B). For C_9 BS is stable and for C_{10} it is unstable and we observe that, BS is stable for all $(w_0, v_0) \in J_1 \cup J_2$, where J_1 and J_2 are connected regions but $J_1 \cup J_2$ is disconnected.

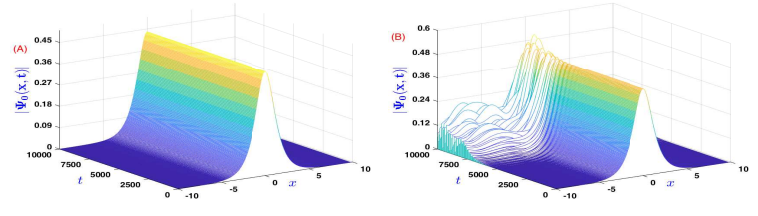


FIG. 11. Excitations of nonlinear localized state of (26) with initial condition (13) in (w_0, v_0) plane for $g = 1$, $\beta = 1$, (A) $v_{01} = 0.731, v_{02} = 0.731, w_{01} = 0.024, w_{02} = -0.024$; (B) $v_{01} = 0.731, v_{02} = 0.731, w_{01} = 0.024, w_{02} = 0.076$.

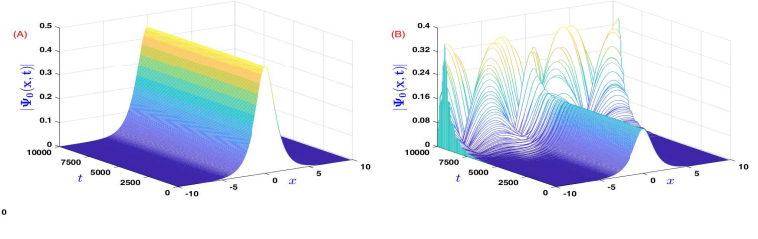


FIG. 12. Excitations of stable nonlinear localized state of (26) with initial condition (13) in (w_0, β) plane for $g = 1$, $v_0 = 0.5$, (A) $\beta_{01} = -1.550, \beta_{02} = -1.550, w_{01} = -0.016, w_{02} = 0.016$; (B) $w_{01} = -0.015, \beta_{01} = 1.43, w_{02} = 0.017, \beta_{02} = 1.44$

Similarly, in (w_0, β) plane for $g = 1$, (w_0, β) plane excitations of BS of (26) along $C_{11} : P_1(-0.016, -1.55) (\in J_4) \rightarrow P_2(0.016, -1.55) (\in J_4)$ and $C_{12} : P_1(-0.015, 1.43) \in J_6 \nearrow P_2(0.017, 1.44) \in I_2$ curves are shown in Fig. 12 (A) and (B) respectively. Here, C_{11} lies in a stable region J_4 of Fig. 7 (D) and for C_{12} , some part lies in a stable region J_6 and the remaining part lies in unstable region I_2 of Fig. 7 (E). One can see that, BS is stable for C_{11} and it is unstable for C_{12} . Similarly, BS is stable in $\cup_{i=3}^6 J_i$.

B. Excitation of DS

In this case, time dependent potential amplitudes $w_0(t)$ and $v_0(t)$ are shown in Fig. 13 (A), for four curves $C_{13} : P_1(-0.2, 0.25) \rightarrow P_2(0.2, 0.25)$; $C_{14} : P_1(-0.2, 0.65) \rightarrow P_2(0.2, 0.65)$; $C_{15} : P_1(-0.2, 0.25) \uparrow P_2(-0.2, 0.32)$; $C_{16} : P_1(-0.2, 0.25) \nearrow P_2(0.2, 0.65)$, and curves are shown in Fig. 13 (B) and excitations of DS of (26) with initial condition (14) along these curves are shown in Fig. 13 (C) - (F), for $g = \beta = \delta = 1$ in (w_0, v_0) plane. One can see that, curves C_{13}, C_{14} and C_{15} are passed through stable modes (blue dots) but C_{16} passes through some stable (blue dots) and unstable modes (magenta dots) and DS is stable along C_{13}, C_{14}, C_{15} and unstable along C_{16} . Therefore, DS is stable in a disconnected \mathcal{PT} unbroken region in (w_0, v_0) plane.

Similarly, excitations of DS of (26) in (w_0, β) plane are evaluated along $(C_{17} : P_1(-0.1, -0.85) \rightarrow P_2(0.1, -0.85); C_{18} : P_1(-0.21, -1.4) \rightarrow P_2(0.21, -1.4); C_{19} : P_1(0.1, 0.85) \nearrow P_2(0.2, 1.15); C_{20} : P_1(-0.1, -0.85) \searrow P_2(0.21, -1.4))$ are shown in Fig. 14 (C) - (F), for $g = 1, v_0 = 0.5, \delta = 1$ and curves are shown in Fig. 14 (B) and the corresponding $w_0(t), \beta(t)$ are shown in Fig. 14 (A). One can see that DS is stable along C_{17}, C_{18}, C_{19} and unstable for C_{20} , where the curve C_{20} passes through stable and unstable modes of DS. Therefore, DS is stable in a disconnected \mathcal{PT} unbroken region in (w_0, β) plane.

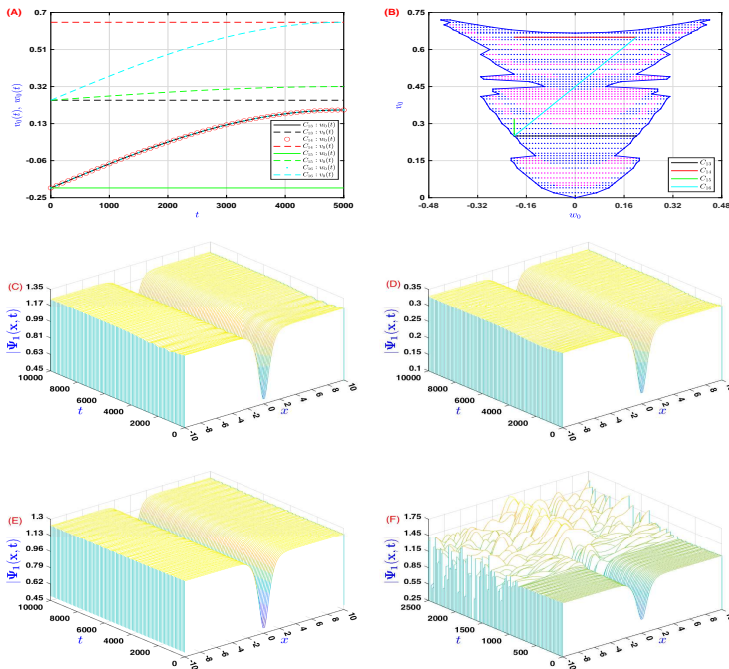


FIG. 13. (A) Shows time dependent potential amplitudes w_0, v_0 for different curves. (B) Shows that stable (*blue dots*) and unstable (*magenta dots*) modes of DS and four curves C_i , $i = 13 - 16$. Excitations of stable-unstable nonlinear delocalized state of (26) with initial condition (14), for $g = 1, \beta = 1, \delta = 1$, (C) $v_{01} = 0.25, v_{02} = 0.25, w_{01} = -0.20, w_{02} = 0.20$; (D) $v_{01} = 0.65, v_{02} = 0.65, w_{01} = -0.20, w_{02} = 0.20$; (E) $v_{01} = 0.25, v_{02} = 0.32, w_{01} = -0.20, w_{02} = -0.20$; (F) $v_{01} = 0.25, v_{02} = 0.65, w_{01} = -0.20, w_{02} = 0.20$.

V. CONCLUSION

In this paper, a cubic NLSE with \mathcal{PT} -symmetric potential has been considered. A bright soliton and a bright-dark soliton interaction are generated in terms of potential amplitudes v_0, w_0 and β . Depending on these parameters, bright-dark soliton interaction reduces to a BS if $w_0^2 > \frac{1}{4\beta^2}$ and a DS, if $w_0^2 < \frac{1}{4\beta^2}$. A phase transition occurs between BS and DS. In addition, \mathcal{PT} broken-unbroken phase transition is shown with respect to w_0, v_0, β and also it is shown in (w_0, v_0) and (w_0, β) planes. The linear stability analysis of BS and DS are investigated and obtained stable regions of BS in \mathcal{PT} broken unbroken region and of DS in \mathcal{PT} unbroken region. We have found that, (i) BS is stable in two connected regions $I_3 \cup J_1 \cup J_2$ (see Fig. 6 (A)) in (w_0, v_0) plane and I_7 (see Fig. 6 (B)) in (w_0, β) plane for $g = -1$. (ii) BS is stable in two disconnected regions $J_1 \cup J_2$ (see Fig. 7 (B)) in (w_0, v_0) plane and $\cup_{i=3}^6 J_i$ (see Fig. 7 (D), (E)) in (w_0, β) plane for $g = 1$. (iii) DS is stable in a small connected re-

gion in (w_0, v_0) plane such that $\frac{2+w_0^2}{3} \leq v_0 \leq \frac{2+w_0^2}{3} + \epsilon$, where $0 \leq \epsilon < 0.1, w_0^2 < \frac{1}{4}$, for $g = -1, \beta = \delta = 1$. (iv) DS is stable in two disconnected regions I_3 (see Fig. 8 (A)) in (w_0, v_0) plane and in I_8 (see Fig. 8 (B)) (w_0, v_0) plane for $g = 1$. (v) Solution (14) is always unstable for $w_0^2 > \frac{1}{4\beta^2}$. All these regions are verified by eigenvalue problem (20), then verified by direct numerical simulation, after that they are verified by excitations of BS and DS of time dependent nonlinear Schrödinger equation with time dependent potential amplitudes. The curves are taken with different length in different directions, which are defined in their

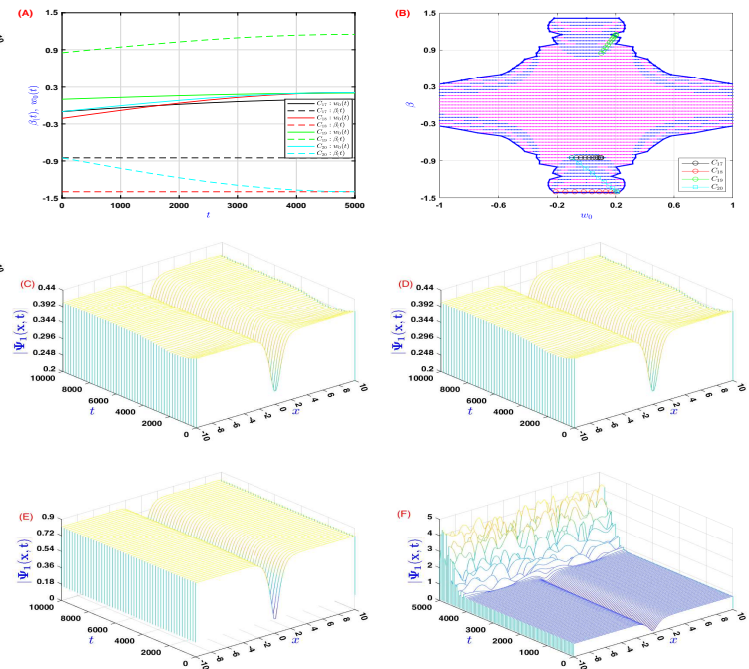


FIG. 14. (A) Shows time dependent potential amplitudes w_0, v_0 for different curves. (B) Shows that stable (*blue dots*) and unstable (*magenta dots*) modes of DS and four curves C_i , $i = 17 - 20$. Excitations of stable-unstable nonlinear delocalized state of (26) with initial condition (14), for $g = 1, v_0 = 0.5, \delta = 1$, (C) $\beta_{01} = -0.85, \beta_{02} = -0.85, w_{01} = -0.10, w_{02} = 0.10$; (D) $\beta_{01} = -1.40, \beta_{02} = -1.40, w_{01} = -0.21, w_{02} = 0.21$; (E) $\beta_{01} = 0.85, \beta_{02} = 1.15, w_{01} = 0.10, w_{02} = 0.20$; (F) $\beta_{01} = -0.85, \beta_{02} = -1.40, w_{01} = -0.10, w_{02} = 0.21$.

pective domain. For examples only twenty excitations are shown along twenty curves C_i , $i = 1 - 20$ and just twelve curves C_i , $i = 1 - 4, 13 - 20$ are shown among them.

ACKNOWLEDGEMENT

Debraj Nath dedicates this article to the memory of his kind brother, late Raj Kumar Nath. Amiya Das gratefully acknowledges financial support from SERB-DST, Govt. of India (EEQ/2017/000150) and DST PURSE-II University of Kalyani.

[1] C. M. Bender and S. Boettcher, Phys. Rev. Lett. **80** (1998) 5243. C. M. Bender, D. C. Brody, H. F. Jones, Phys. Rev. Lett. **89** (2002) 270401. C. M. Bender, S. Boettcher, P. N. Meisinger, J. Math. Phys. **40** (1999) 2201. C. M. Bender, Rep. Prog. Phys. **70** (2007) 947.
[2] K. G. Makris, R. El-Ganainy, D. N. Christodoulides, Z. H. Musslimani, Phys. Rev. A **81** (2010) 063807.

[3] C. E. Ruter, K. G. Makris, R. El-Ganainy, D. N. Christodoulides, M. Segev, D. Kip, Nat. Phys. **6** (2010) 192. A. Guo, G. J. Salamo, D. Duchesne, R. Morandotti, M. Volatier-Ravat, V. Aimez, G. A. Siviloglou, D. N. Christodoulides, Phys. Rev. Lett. **103** (2009) 093902. Z. Lin, H. Ramezani, T. Eichelkraut, T. Kottos, H. Cao, D. N. Christodoulides, Phys. Rev. Lett. **106** (2011) 213901.

- [4] Z. H. Musslimani, K. G. Makris, R. El-Ganainy and D. N. Christodoulides, *Phys. Rev. Lett.* **100** (2008) 030402.
- [5] M. V. Berry, *J. Phys. A* **41** (2008) 244007.
- [6] S. Longhi, *Phys. Rev. Lett.* **103** (2009) 123601.
- [7] O. Bendix, R. Fleischmann, T. Kottos and B. Shapiro, *J. Phys. A* **43** (2010) 265305.
- [8] K. G. Makris, Z. H. Musslimani, D. N. Christodoulides and S. Rotter, *Nat. Commun.* **6** (2014) 7257.
- [9] J. Schindler, Z. Lin, J. M. Lee, H. Ramezani, F. M. Ellis and T. Kotto, H. Ramezani, F. M. Ellis and T. Kotto, *J. Phys. A* **45** (2012) 444029.
- [10] H. Cartarius and G. Wunner, *Phys. Rev. A* **86** (2012) 013612.
- [11] E.-M. Graefe, *J. Phys. A* **45** (2012) 444015.
- [12] D. Dast, D. Haag, H. Cartarius, J. Main and G. Wunner, *J. Phys. A* **46** (2013) 375301.
- [13] G. Castaldi, S. Savoia, V. Galdi, A. Al'u and N. Engheta, *Phys. Rev. Lett.* **110** (2013) 173901.
- [14] N. Lazarides and G. P. Tsironis, *Phys. Rev. Lett.* **110** (2013) 053901.
- [15] M. Kang, F. Liu and J. Li, *Phys. Rev. A* **87** (2013) 053824.
- [16] H. Alaeian and J. A. Dionne, *Phys. Rev. A* **89** (2014) 033829.
- [17] G. P. Tsironis and N. Lazarides, *App. Phys.* **115** (2014) 449.
- [18] T. Kottos, *Nat. Phys.* **6** (2010) 166.
- [19] C. E. Rüter, K. G. Markis, R. El-Ganainy, D. N. Christodoulides, M. Segev and D. Kip, *Nat. Phys.* **6** (2010) 192.
- [20] L. Feng et al., *Nature Mater.* **12** (2013) 108.
- [21] J. Schindler, A. Li, M. C. Zheng, F. M. Ellis and T. Kottos, *Phys. Rev. A* **84** (2011) 040101(R).
- [22] K. G. Makris, R. El-Ganainy, D. N. Christodoulides, *Phys. Rev. Lett.* **100** (2008) 103904. A. Ruschhaupt, F. Delgado, J. G. Muga, *J. Phys. A: Math. Gen.* **38** (2005) L171. R. El-Ganainy, K. G. Makris, D. N. Christodoulides, Z. H. Musslimani, *Opt. Lett.* **32** (2007) 2632. M. V. Berry, *J. Phys. A: Math. Theor.* **41** (2008) 244007. S. Klaiman, U. Gunther, N. Moiseyev, *Phys. Rev. Lett.* **101** (2008) 080402. S. Longhi, *ibid.* **103** (2009) 123601. S. Longhi, *Phys. Rev. A* **82** (2010) 031801(R). H. Ramezani, D. N. Christodoulides, V. Kovanis, I. Vitebskiy, T. Kottos, *Phys. Rev. Lett.* **109** (2012) 033902. M. A. Miri, A. Regensburger, U. Peschel, D. N. Christodoulides, *Phys. Rev. A* **86** (2012) 023807.
- [23] A. Guo, G. J. Salamo, D. Duchesne, R. Morandotti, M. Volatier-Ravat, V. Aimez, G. A. Siviloglou, D. N. Christodoulides, *Phys. Rev. Lett.* **103** (2009) 093902. C. E. Reuter, K. G. Makris, R. El-Ganainy, D. N. Christodoulides, M. Segev, D. Kip, *Nat. Phys.* **6** (2010) 192. A. Regensburger, C. Bersch, M.-A. Miri, G. Onishchukov, D. N. Christodoulides, U. Peschel, *Nature* **488** (2012) 167.
- [24] A. Khare, S. M. Al-Marzoug, H. Bahlouli, *Phys. Lett. A* **376** (2012) 2880.
- [25] D. A. Zezyulin, V. V. Konotop, *Phys. Rev. A* **85** (2012) 043840.
- [26] B. Midya, R. Roychoudhury, *Phys. Rev. A* **87** (2013) 045803.
- [27] S. Hu, X. Ma, D. Lu, Z. Yang, Y. Zheng, W. Hu, *Phys. Rev. A* **84** (2011) 043818.
- [28] S. Hu, G. Liang, S. Cai, D. Lu, Q. Guo, W. Hu, *arXiv:1203.1862v1* (2012)
- [29] C. P. Jisha, L. Devassy, A. Alberucci, V. C. Kuriakose, *Phys. Rev. A* **90** (2014) 043855.
- [30] B. Midya, *Nonlinear Dyn.* **79** (2015) 409.
- [31] P. Li, B. Liu, L. Li, D. Mihalache, *Rom. J. Phys.* **61** (2016) 577.
- [32] P. Li, L. Li, D. Mihalache, *arXiv:1804.02629v1 [physics.optics]* (2018).
- [33] Z. C. Wen, Z. Yan, *Phys. Lett. A* **379** (2015) 2025.
- [34] Y. Chen, Z. Yan, *Commun. Nonlin. Sc. Numer. Simulat.* **57** (2018) 34.
- [35] N. N. Akhmediev and A. Ankiewicz, *Solitons: Nonlinear pulses and beams* (Chapman and Hall, London, 1997)
- [36] Y. S. Kivshar and G. P. Agrawal, *Optical Solitons: From Fibers to Photonic Crystals* (Academic, San Diego, 2003).
- [37] Z. H. Musslimani, K. G. Makris, R. El-Ganainy and D. N. Christodoulides, *J. Phys. A* **41** (2008) 244019.
- [38] K. G. Makris, R. El-Ganainy, D. N. Christodoulides and Z. H. Musslimani, *Int. J. Theo. Phys.* **50** (2011) 1019.
- [39] F. Kh. Abdullaev, V. V. Konotop, M. Salerno and A. V. Yulin, *Phys. Rev. E* **82** (2010) 056606.
- [40] A. Khare, S. M. Al-Marzoug and H. Bahlouli, *Phys. Lett. A* **376** (2012) 2880.
- [41] V. Achilleos, P. G. Kevrekidis, D. J. Frantzeskakis and R. Carretero-González, *Phys. Rev. A* **86** (2012) 013808.
- [42] A. Khare and A. Saxena, *Phys. Lett. A* **377** (2013) 2761.
- [43] M. Salerno, *J. Geom. Symm. Phys.* **32** (2013) 25.
- [44] T. Mayteevarunyoo, B. A. Malomed and A. Reksabutr, *Phys. Rev. E* **88** (2013) 022919.
- [45] H. Xu, P. G. Kevrekidis, Q. Zhou, D. J. Frantzeskakis, V. Achilleos and R. Carretero-González, *Rom. J. Phys.* **59** (2014) 185.
- [46] B. Midya and R. Roychoudhury, *Ann. Phys.* **341** (2014) 12.
- [47] H. Chen, S. Hu and L. Qi, *Opt. Commun.* **331** (2014) 139.
- [48] V. V. Konotop and D. A. Zezyulin, *Opt. Express* **39** (2014) 553.
- [49] A. K. Sarma, M.-A. Miri, Z. H. Musslimani and D. N. Christodoulides, *Phys. Rev. A* **89** (2014) 052918.
- [50] C.-Q. Dai and Y. -Y. Wang, *Opt. Commun.* **315** (2014) 303.
- [51] I. Göskel, N. Antar and I. Bakirtas, *Opt. Commun.* **354** (2015) 277.
- [52] Z. Yan, Z. Wen and C. Hang, *Phys. Rev. E* **92** (2015) 022913.
- [53] D. Nath, B. Roy, R. Roychoudhury, *Chaos, Solitons & Fractals* **81** (2015) 91.
- [54] A. Das, N. Ghosh and D. Nath, *Phys. Lett. A* **384** (2020) 126681.
- [55] D. Nath and P. Roy, *J. Nonlinear Optic. Phys. Mat.* **25** (2016) 1650036.
- [56] D. Nath and P. Roy, *Phys. of Part. and Nuclei Lett.* **14** (2017) 347.
- [57] F. Cooper, A. Khare and U. Sukhatme, *Supersymmetry in Quantum Mechanics*, World Scientific (2001).
- [58] Y.S. Kivshar, B. Luther-Davies, *Phys. Rep.* **298** (1998) 81197. R. Heidemann, S. Zhdanov, R. Stterlin, H.M. Thomas, G.E. Morfill, *Phys. Rev. Lett.* **102** (2009) 135002. T. Xu, B. Tian, L.L. Li, X. Lv, C. Zhang, *Phys. Plasmas* **15** (2008) 102307. T. Tsurumi, M. Wadati, *J. Phys. Soc. Jpn.* **97** (1998) 2294. M. Wadati, N. Tsuchida, *J. Phys. Soc. Jpn.* **75** (2006) 014301. D. Mandelik, R. Morandotti, J.S. Aitchison, Y. Silberberg, *Phys. Rev. Lett.* **92** (2004) 093904.
- [59] Z. Shi, X. Jiang, X. Zhu and H. Li, *Phys. Rev. A* **84** (2011) 053855.
- [60] Z. Ahmed, *Phys. Lett. A* **282** (2001) 343.
- [61] J. Yang, *Nonlinear Waves in Integrable and Nonintegrable Systems* (SIAM, Philadelphia, 2010).
- [62] S. Nixon, L. Ge and J. Yang, *Phys. Rev. A* **85** (2012) 023822.
- [63] D. A. Zezyulin, Y. V. Kartashov and V. V. Konotop, *Euro. Phys. Lett.* **96** (2011) 64003.
- [64] D. Nath, B. Roy, R. Roychoudhury, *Opt. Commun.* **393** (2017) 224.
- [65] D. Nath, N. Saha, B. Roy, *Eur. Phys. J. Plus* **133** (2018) 504.
- [66] M. Vakhitov and A. Kolokolov, *Radiophys. Quantum Electron.* **16** (1973) 783.
- [67] W. Bao, Q. Tang, and Z. Xu, *J. Comput. Phys.* **235** (2013) 423. D. Nath, Y. Gao, R.B. Mareeswaran, T. Kanna, and B. Roy, *Chaos* **27** (2017) 123102.
- [68] Z. Yan, Y. Chen, *Chaos* **27** (2017) 073114. Z. Yan, Z. Wen, V. V. Konotop, *Phys. Rev. A* **92** (2015) 023821. Y. Chen and Zhenya Yan, *Phys. Rev. E* **95** (2017) 012205. Y. Chen and Z. Yan, *Scientific Reports* **6**:23478 DOI: 10.1038/srep23478, (2016); Y. Chen, Z. Yan, D. Mihalache and B. A. Malomed, *Scientific Reports* **7**: 1257 DOI:10.1038/s41598-017-01401-3, (2017).